Measurements on thin-film high-T_c superconductors

by A. Kapitulnik
K. Char

We report on the fabrication and properties of high-T_c superconducting films, and discuss the possible origin of the linear resistivity. We further discuss the c-axis conductivity. We present data to show that the coherence length is 12 Å parallel to the plane and 2 Å perpendicular to the plane in the superconducting state. Tunneling data show that the energy gap is large, with $2\Delta/kT_c \approx 7$.

1. Introduction

Thin films of high-temperature superconductors (HTSC) are useful for many measurements of physical properties such as optical transmittance and tunneling. For anisotropic materials, where physical properties depend on the direction, well-oriented films can be an important tool for measuring anisotropic transport properties.

To date, many methods have been employed for the successful synthesis of thin HTSC films. Of all the known high-T_c phases, the one most studied is $YBa_2Cu_3O_{7-\delta}$ (123). We therefore concentrate in this paper on the synthesis and properties of Y–Ba–Cu–O films. The film stoichiometry will vary as we explore the phase diagram in the vicinity of the 123 phase (see **Figure 1**).

There are two major methods of film synthesis—*in situ* growth and postannealing. If we regard *in situ* growth as genuinely epitaxial, postannealing (in which the constituents are placed on the substrate in an amorphous form) is a solid-state epitaxial method.

In this paper we discuss films prepared by the postannealing method [1–5]. For a recent discussion on *in situ* deposition, see for example the paper by Missert et al. [6].

We studied films having excellent superconducting properties, ranging in thickness from 500 Å to 5 μm, and deposited on $SrTiO_3$ substrate. The dependence of their orientation on parameters such as composition, annealing condition, and film thickness is discussed. In particular, we compare properties of the 123 phase with the Cu-rich phase $Y_2Ba_4Cu_8O_{16}$ (248). **Table 1** is a summary of the properties of films of these two phases with yttrium, or with erbium substituting for yttrium. The source for the quoted numbers is discussed in the text, and the relevant references are mentioned.

2. Film preparation

• *Deposition*

We describe below primarily the magnetron gun co-sputtering method. The other method used was e-beam co-evaporation with a BaF_2 source instead of pure Ba. This technique was first introduced by Mankiewich et al. and is described in [7]. Y, Ba, and Cu metals were melted and then machined into targets 5 cm in diameter and 4 mm thick. As described in [1], three sputtering guns with the targets

mounted were set up in a triangular arrangement and angled to point toward the center of the sample holder. Three rows of seven 6 × 6-mm substrates were mounted at each run, located 12 cm above the targets. This arrangement provided a composition spread in which each row differs by the copper content and the Y/Ba ratio. A typical composition spread when aiming at 123 material is shown in Figure 1. The composition varied between two adjacent substrates by about 0.5 atomic %. The base pressure of the chamber was 1 × 10^{-6} torr. Ar gas at 2 × 10^{-3} torr was introduced at the Ba and Y sources to provide the plasma and at the same time flush them and prevent rapid oxidation. Oxygen was introduced at the substrate using specially designed slits [1] at a partial pressure of 1 × 10^{-4} torr. With that arrangement, stable and reproducible depositions could be achieved. The substrate temperature during deposition varied from ambient temperature to 400°C. No dramatic effects were observed due to differing substrate temperatures.

Y and Cu were dc-sputtered, whereas Ba was rf-sputtered. The Ba target was presputtered until the plasma turned bright green, an indication that the target was no longer covered with an oxide layer. The rate from each source was set by a single quartz-crystal monitor, placed just below the gas inlet system [1]. The combined rate was checked with all the guns and the oxygen source in operation. The deposition rate was 3–4 Å/s.

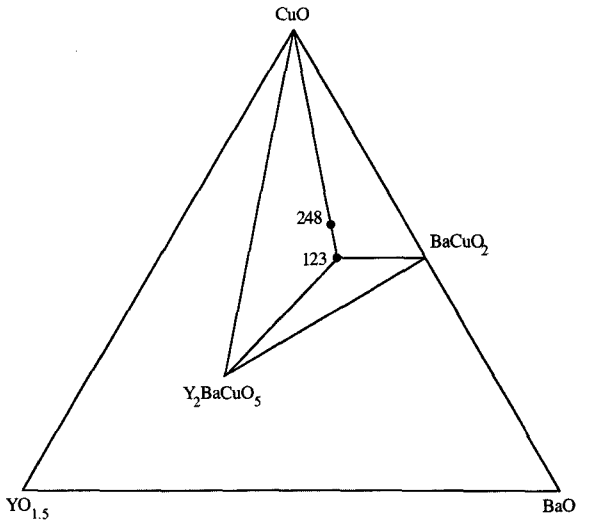

Figure 1

Ternary phase diagram of Y–Ba–Cu–O (for fixed O).

• *Growth*

As mentioned above, films were postannealed after deposition. A high degree of orientation was achieved by solid-state epitaxial growth. Returning to Figure 1, we note the important points in the growth procedure. In general, the composition of a film before annealing is the most important factor. $YBa_2Cu_3O_{7-\delta}$ is a line compound (or a point compound when the oxygen stoichiometry is fixed); any deviation from the stoichiometry results in secondary phases. Nevertheless, since the growth is induced by the substrate at elevated temperatures after deposition, one can think of starting with off-stoichiometric material and use the excess material as flux, as is the case with single-crystal growth. Excess material can also affect the matching of the growing film with the substrate (e.g., by relieving strain) and hence

Table 1 Summary of typical properties of 123 and 248 films.

	123	*248*
Structure		
c	11.7 Å	27.2 Å (13.6 Å)
a–b	0.07 Å	0.015 Å
Normal state		
ρ (100 K)	80–150	20–60 μΩ-cm
$(d\rho/dt)$	1 μΩ-cm/K	0.75 μΩ-cm/K
R_H^{-1} (100 K)	~3 × 10^{21}/cm^3 (0.52/unit cell of 123)	~1.6 × 10^{22}/cm^3 (3.25/unit cell of 124)
Superconducting state		
T_c (ΔT)	90 K (0.5 K)	81 K (0.5 K)
J_c (4.2 K) by magnetization	>2 × 10^7 A/cm^2	>2 × 10^7 A/cm^2 (EBCO)
J_c (77 K)	>2 × 10^6 A/cm^2	—
R_s (4.2 K)* 150 GHz	15 mΩ	15 mΩ
S_Φ (4.2 K)†	<10^{-9} Φ_0/Hz	—
U_0 (pinning energy)‡	~0.2–0.4 eV	~0.4 eV

* [38]. † [39]. ‡ [40].

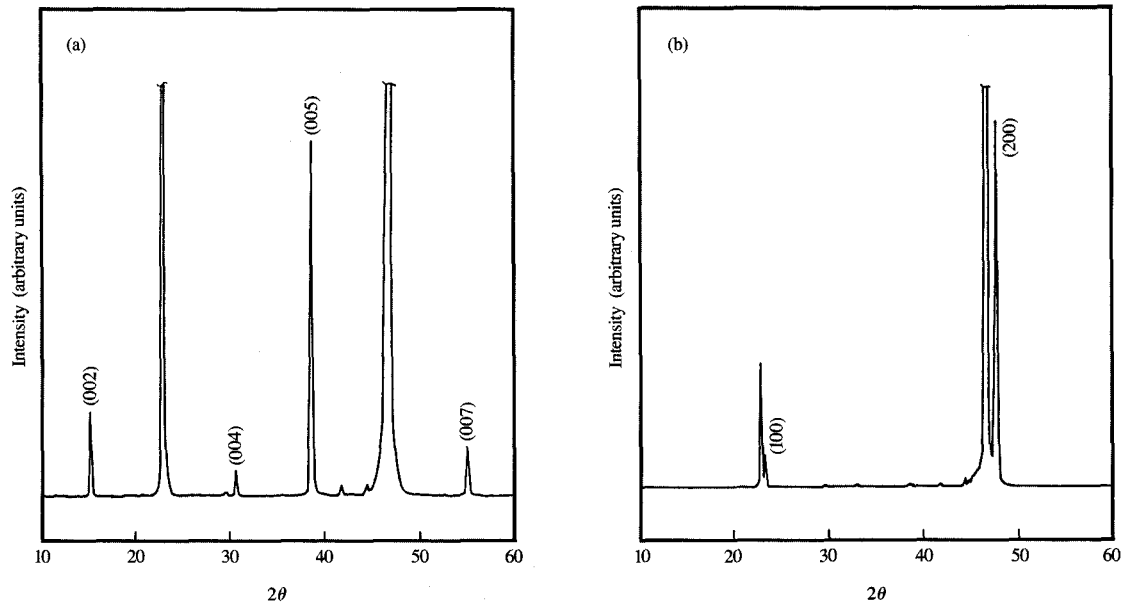

Figure 2

Typical X-ray scattering from $YBa_2Cu_3O_{7-\delta}$: (a) *c*-axis film; (b) *a*-axis film. (The two peaks which are not indexed are from the substrate.)

Table 2 Conditions for the specific orientation of films on $SrTiO_3$.

	c-axis orientation	*a-axis orientation*
Cu composition	Cu-poor	Cu-rich
Y/Ba composition	Ba-rich	Y-rich
Thickness	<4000 Å	>4000 Å
Anneal	More than 1 h at 850°C	1 h at 850°C

can control the orientation of the film. Good films on $SrTiO_3$ have been reported by many groups. These films are almost exclusively *c*-axis-oriented. Note, however, that below 600°C, from the point of view of lattice constant matching, this is not the preferred orientation. Thus the *c*-axis film is expected to contain a large number of defects.

We have mentioned that the orientation of the films can be controlled, in particular by adjusting their nominal composition. **Table 2** summarizes these findings. **Figure 2** shows X-ray diffraction data which represent *a*-axis- and *c*-axis-oriented films. On the basis of the X-ray diffraction-line intensity, one can roughly estimate the amount of *c*-axis orientation vs. *a*-axis orientation by comparing the height of the {005} X-ray diffraction line to 70% of the height of the {200} line, respectively.

According to the X-ray data, films as deposited are basically amorphous. They are subsequently annealed for 3 h at 650°C followed by annealing for 1 h at 750°C and 1 h at 850°C. The result is an *a*-axis film (depending on stoichiometry, as noted above). With further annealing or annealing up to 880°C, *c*-axis orientation appears.

It is important to note that in *c*-axis films with Cu-poor and Ba-rich composition, a small fraction of $BaCuO_2$ ($2\theta \sim 29.8°$) often grows epitaxially [8].

We turn now to the 248 phase, which was discovered [9, 10] during the analysis of X-ray data on *c*-axis films with Cu-rich nominal stoichiometry. Extra diffraction lines that could be indexed with a new phase having a *c*-parameter of 27.2 Å were discovered. The structure of this phase was modeled using the defect structure discovered by Zandbergen et al. [11] in bulk materials. This phase has an additional Cu–O chain layer between two regular 123 unit cells, shifted by half a lattice constant. Detailed structural properties of the 248 phase are found in [12]. It is important to note, however, that the orthorhombic distortion of this phase is much smaller than in the 123 phase, and it is not as sensitive to oxygen loss (the oxygen in the chains is locked, as in $SrCuO_2$). **Figure 3** shows X-ray data and the crystal

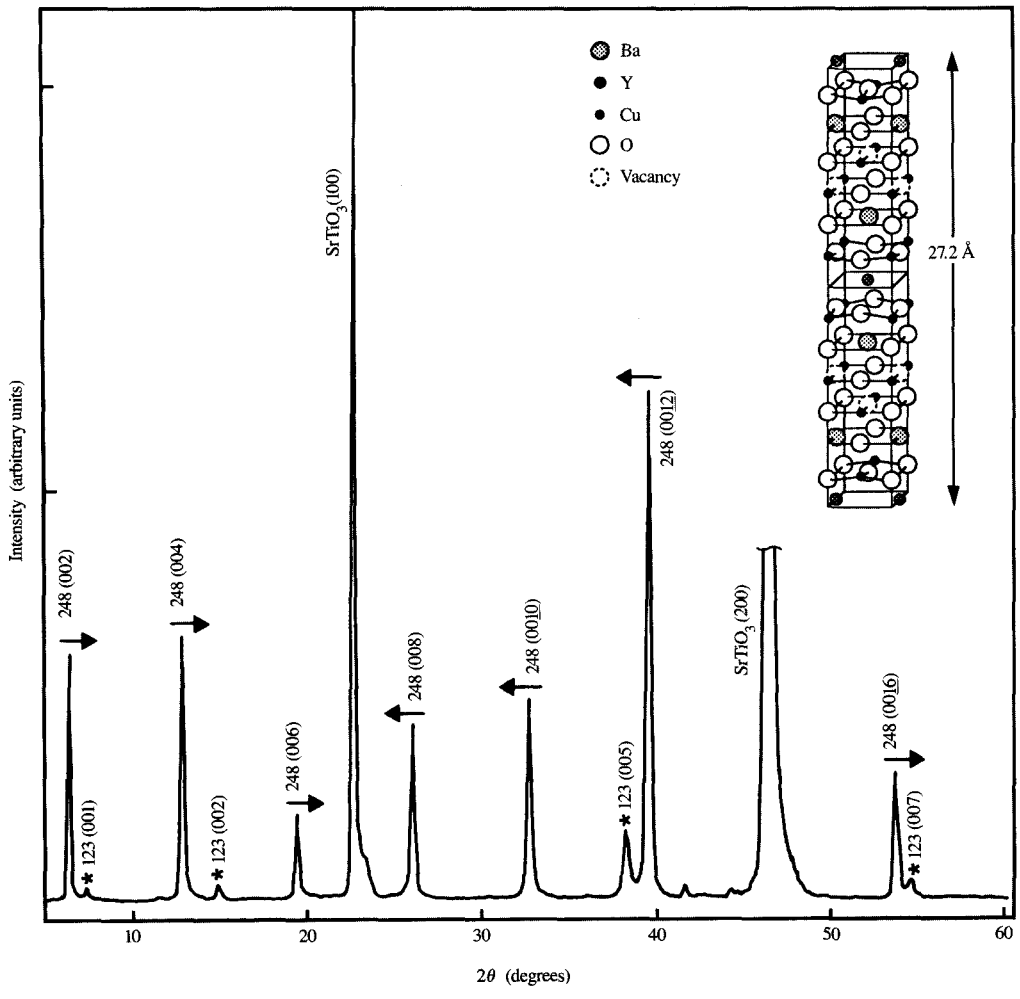

Figure 3

Crystal structure and X-ray pattern (c-axis) of $Y_2Ba_4Cu_8O_{16}$.

structure of the 248 phase. Quite remarkably, the procedures described above for the preparation of 123 and 248 films based on Y material apply to Er as well. In fact, the structure of the 248 phase was determined unambiguously by studying in parallel the two isostructural materials $Y_2Ba_4Cu_8O_{16}$ and $Er_2Ba_4Cu_8O_{16}$ [12].

To conclude this section, we note the difference in morphology of the various types of films. In general, the growth in the direction perpendicular to the c-axis predominates, whereas the substrate induces c-axis growth; c-axis films cannot be grown with good quality thicker than 4000 Å, because a-axis inclusions take over the growth and dominate at large thicknesses. Moreover, we note that in order to control the orientation of the film, slight off-stoichiometry is required. We have found that most of the excess material goes to the surface, leaving the bulk of the film with a relatively pure single phase.

3. Physical properties

Some of the important physical properties of the films which already have been summarized in Table 1 are discussed below. It is important to note that the numbers quoted in Table 1 are typical and highly reproducible. Better characteristics are often found.

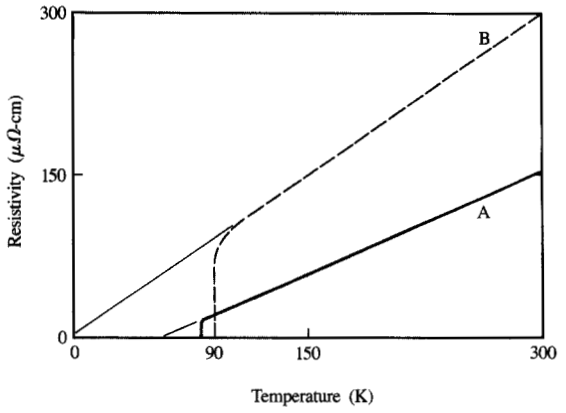

Figure 4

Temperature dependence of resistivity of 248 phase (curve A), and 123 phase (curve B).

Normal state

Both phases 123 and 248 exhibit linear resistivity from room temperature down to T_c. The value of ρ and its slope for the films is similar to what is regularly found in the best single crystals available. A similar observation can be made for measurements of the Hall coefficient and the thermoelectric power. We discuss below two of the important properties, the linear resistivity and the anisotropy in the optical reflectance.

Linear resistivity

One of the most fascinating properties of the high-T_c superconductors is the linear dependence of the resistivity on temperature. Sometimes the resistivity appears linear up to ~1000 K [13]. Although several new models were proposed to explain this effect, we argue below that the linear resistivity can arise from simple electron–phonon scattering.

For a good metal, the resistivity at low temperature will be $\rho = \rho_i + aT^2 + bT^5$, where ρ_i is the impurity-scattering (residual) resistivity, a is the electron correlation coefficient, and b is the coefficient of the electron–phonon term (Bloch–Gruneisen). At high temperatures, above θ_D, $\rho = \rho_i + AT$, where A is proportional to the electron–phonon coupling constant. At low temperatures very often the T^2 term is larger than the T^5 term and thus is mostly observed. However, at intermediate temperatures ($0.1 \leq T \leq \theta_D$), a crossover regime for the Bloch–Gruneisen formula exists which is extremely linear, but since it connects the T^5 term at low temperatures to the T term at high temperatures, it obeys $\rho \sim \rho_0 + CT$ such that $\rho_0 < 0$. An example can be found in Ziman [14]. For an ordinary metal with θ_D ~200–300 K, this intermediate regime can extend to ~150–200 K. If, on the other hand, the material is anisotropic, such that the electrons interact with fewer phonon modes, this crossover point can increase, for the simple reason that an effective, higher Debye temperature appears for the kinetic coefficients. If, e.g., the thermodynamic Debye temperature $\theta_D \approx 500$ K, as for the oxides, but the electrons do not interact with transverse phonons, the effective sound velocity will increase by the following ratio (assuming for the elastic coefficients $C_{11} \sim 3C_{44}$ and a cubic symmetry): $[1 + 2(C_{11}/C_{44})^{3/2}]^{1/3} \approx 2.25$. Thus, the effective Debye temperature will be $\sim 500 \times 2.25 = 1125$ K. A crossover to the high-temperature regime will occur at ~800 K. Thus, a linear resistivity that intersects the resistivity axis as a negative value is expected. Indeed, some quasi-two- and one-dimensional systems exhibit this kind of behavior [15]. In the high-T_c family the "248" material clearly shows this behavior (**Figure 4**) and might indicate that the linear resistivity of all the high-T_c materials originates in that intermediate regime. It certainly indicates that most high-T_c materials are so disordered that this residual resistivity is high—it brings the whole curve up such that positive crossing of the resistivity axis occurs.

Finally, we should note that at higher temperatures optical phonons (Einstein modes) will appear and bend the resistivity curve upward, resulting in less pronounced crossover between the two linear-T regimes. All these effects will result in a smooth linear resistivity from very low temperatures to very high temperatures.

Anisotropy

Examination of the crystal structure of all high-T_c materials indicates a strong anisotropy. Since one expects the electronic wave functions to overlap strongly in the Cu–O planes, it implies the highest conductivity in the a–b plane. The anisotropy which is evident in the crystal structure and is expected in the physical properties is harder to extract in thin films. Although high-quality a-axis films can be fabricated, they are not single crystals. The c-axis that lies in the plane can point in two different directions with respect to the substrate. Any electronic transport for these kinds of films will choose its path through a–b planes, thus almost completely avoiding c-axis transport. We thus expect the resistivity in a-axis films to be a superposition of highly percolative a–b resistivity with some c-axis resistivity component.

Some reports have attempted to prove not only that the high-T_c cuprates are highly anisotropic, but also that they exhibit semiconducting behavior in the c-direction [16, 17]. As materials preparation has improved, a few recent reports have indicated the disappearance of this behavior and the appearance of a metallic conductivity along the c-axis with temperature dependence similar to that in the a–b plane but with much smaller magnitude [18, 19].

It is very important to examine these experimental facts. If indeed the intrinsic behavior is semiconducting, it is quite possible that defects such as grain boundaries and twin boundaries enable a percolation process that is dominated by a–b-plane conduction. The small magnitude of the conductivity is then a result of the percolative nature of the path. On the other hand, this possibility is very difficult to reconcile with the fact that better single crystals show less of this semiconducting behavior.

It is thus desirable to look into individual domains and examine the existence of the intrinsic anisotropy. An optical probe is the most powerful tool for this purpose.

Mid-IR reflectance of single crystals [20] was obtained with a Digilab FTS-40 FTIR spectrometer coupled to a Spectratech IR-PLAN microscope that provided spatial resolution of 50 μm. Single crystals were grown at Princeton University by the flux method in an oxygen flow. Typical crystals were $0.5 \times 0.5 \times 0.1$ mm and had faces of high optical quality and sharply defined edges. Typical T_c's were 91–93 K with 0.5 K transition width. **Figure 5** shows polarized reflectance data from the single crystal together with reflectance data from a (pristine) c-axis-oriented thin film. The similarity between $R_\parallel$ and $R_\perp$ is evident. R_a and R_c represent reflectance data calculated from ε_1 and ε_2 measured by the ellipsometry method. The important feature to notice is the strong upturn of the reflectance at low frequencies as the frequency decreases. Attributing this feature to free carriers, we identify a plasma frequency along the c-axis: $\omega_p^\perp \approx 0.4$ eV. The plasma frequency of the free carriers in the plane is $\omega_p^\parallel \approx 1.6$ eV. The anisotropy is thus

$$(\omega_p^\parallel/\omega_p^\perp)^2 \approx (1.6/0.4)^2 \approx 16.$$

There are two points to be noted. The first is the existence of free carriers along the c-axis, in contradiction to the dc measurements. Of course, one might suggest that the carriers are free at high frequencies but freeze at low frequencies (lower than 80 meV $\approx$ 1000 K); unfortunately, lower frequencies are not available with our instrumentation. The second important issue is that the anisotropy is smaller than that measured in direct current by roughly a factor of four. In fact, it is interesting to note that recent analysis of reflectivity data suggesting strong coupling to some excitations (e.g., magnons) at low frequencies implies an increase of the effective mass by roughly the same factor. Recent measurements of the penetration depth by μSR suggest a similar ratio for $(\lambda^\parallel/\lambda^\perp)^2$ [21]. This is expected in the London theory, where $\omega_p = c/\lambda$.

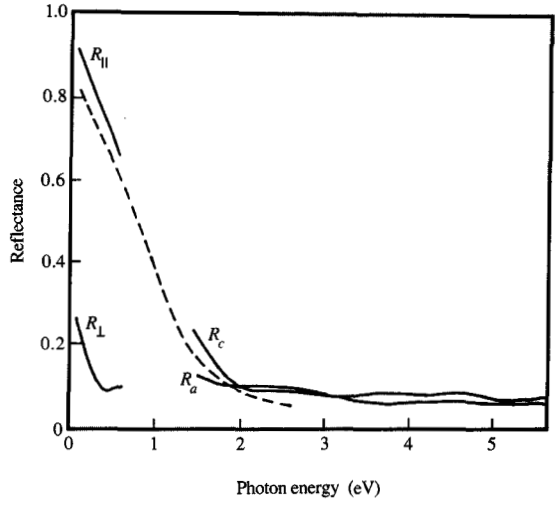

Figure 5

Reflectivity data from 123 phase single crystal. $R_\parallel$ is polarized in the a–b plane and $R_\perp$ is polarized along the c direction. R_a and R_c represent reflectivity from a-axis and c-axis films, respectively, as calculated from ellipsometry data. The dashed line indicates reflectivity from a (pristine) 5000-Å film.

• *Superconducting properties*

One of the most important properties, especially for applications, is the critical current. Good films exhibit high J_c, as listed in Table 1. Most of the measurements were made using the magnetization technique and the so-called Bean's formula [22]. The experimental proof that this formula is indeed valid for high-T_c films was given in [23]. In fact, like many other laboratories, we have found that the better the film quality, the higher its critical current density.

We discuss below two aspects of the superconducting state, coherence length and tunneling measurements.

Fluctuation conductivity, H_{c2}, and coherence length

The extraction of the coherence lengths via the determination of H_{c2} from resistive transitions is not easy in HTSC. In general, because the resistive transition is governed by flux creep [24], a method to analyze field dependence is necessary in order to extract the coherence lengths. A typical set of resistive transitions in parallel and perpendicular fields (i.e., parallel or perpendicular to the a–b plane) is given in **Figure 6**. It is important to note the very small magnetoresistance above the transition in contrast to the huge effect below the zero-magnetic-field transition temperature T_0.

Fluctuation conductivity measurements (at zero magnetic field) indicate that high-T_c materials can be looked at as quasi-two-dimensional conductors. There is an excellent fit to the Lawrence–Doniach theory [25] of fluctuation conductivity in the a–b plane.

At a temperature T near T_c, a contribution σ' adds to the normal-state conductivity $\sigma_n(T)$ which is proportional to T^{-1}

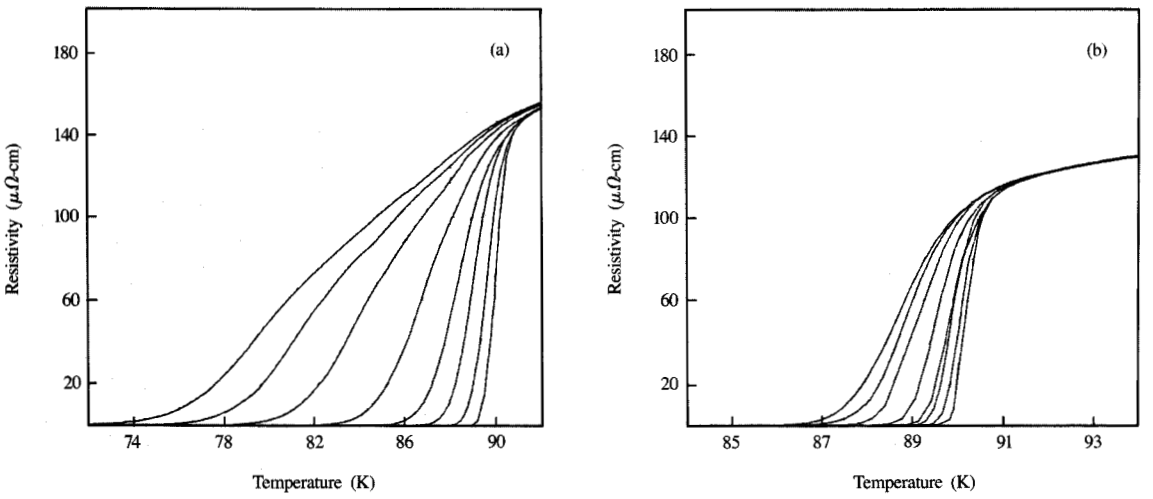

Figure 6

Resistive transitions in magnetic field for *c*-axis 123 phase film: (a) perpendicular field; (b) parallel field. Fields (from right to left): 0 T, 0.2 T, 0.5 T, 1 T, 2 T, 4 T, 6 T, and 8 T.

such that the total conductivity diverges at T_c. Within the Lawrence–Doniach (LD) theory, the fluctuation-enhanced conductivity in the a–b plane is

$$\sigma'(\varepsilon) = Ce^2\{1 + [2\xi_c(0)/s]^2\varepsilon^{-1}\}^{-1/2}/16\varepsilon sh,$$

where $\varepsilon = T/T_c - 1$ and s is the layer periodicity. In this equation we note that σ' will diverge as $\varepsilon^{-1/2}$, which is the 3D behavior, but as we go further, higher than T_c a 2D behavior proportional to ε^{-1} takes place. A dimensionality crossover will occur at a temperature $\sim T_c\{1 + [2\xi_c(0)/s]^2\}$. We note that the LD theory predicts $C = 1$. Our experimental data, however, fit the LD formula with C larger than one. In fact, C can be as large as 10 for highly disordered ceramic materials and of order 2 for cleaner, high-quality films. The interpretation of C is very simple. It states that only $1/C$ of the material fluctuates to contribute to the observed σ'. The important factor is that for any type of sample, $1/C \cdot d\rho/dT$ is a constant ~0.55, no matter what ρ is. This of course predicts an intrinsic resistivity of 55 $\mu\Omega$-cm at 100 K. Indeed, all samples of $YBa_2Cu_3O_7$ show resistivity higher than that value.

As sample quality improves, a lifetime contribution due to the inertia of the paired electrons as they go to the normal state, the so-called Maki–Thomson [27] term, is needed. This term for the quasi-two-dimensional layered materials was calculated by Hikami and Larkin (HL) [28]. Using a pair-breaking rate of $\tau^{-1} \sim T$ to agree with the normal-state resistivity, we find an excellent agreement with this theory, with the factor C being close to 1. In fact, we find our best samples with $C \sim 1.2$. Indeed, in agreement with other measurements that find parts of the materials being degraded, all the fits, either of the dirtier materials with large C or the cleaner, with C approaching 1, agree with the result $\xi_c(0) \simeq 2$ Å and periodicity $s = 11.7$ Å—the unit cell size.

Returning to the coherence length issue, we note that if indeed the broadening of the transition were due to flux creep, we would expect less of this effect far from the resistance point. In fact, if we investigate the H_{c2} determination from a higher and higher fraction of the normal-state resistivity, we find that a definition of H_{c2} close to the onset is indeed linear, and it has the most curvature when it is determined by zero resistance. We found H_{c2} $(\rho = 0) \propto (T_c - T)^{4/3}$ [26]. Measuring H_{c2} by the 90% of ρ_{normal} criteria, where indeed $H_{c2} \propto (T_c - T)$ as expected for a mean-field theory, we find $\xi(0)^{\perp} \approx 2$ Å and $\xi(0)^{\parallel} \approx 12$ Å. This implies an anisotropy of ~36—again, a smaller anisotropy than implied by the ratio of the normal-state resistivities.

Tunneling

Many tunneling results have been published to date [30, 31]. The desire to obtain good tunneling stems from the fact that tunneling studies have historically constituted one of the most powerful probes of the nature of superconductivity and its underlying mechanism. In particular, the derivative of the

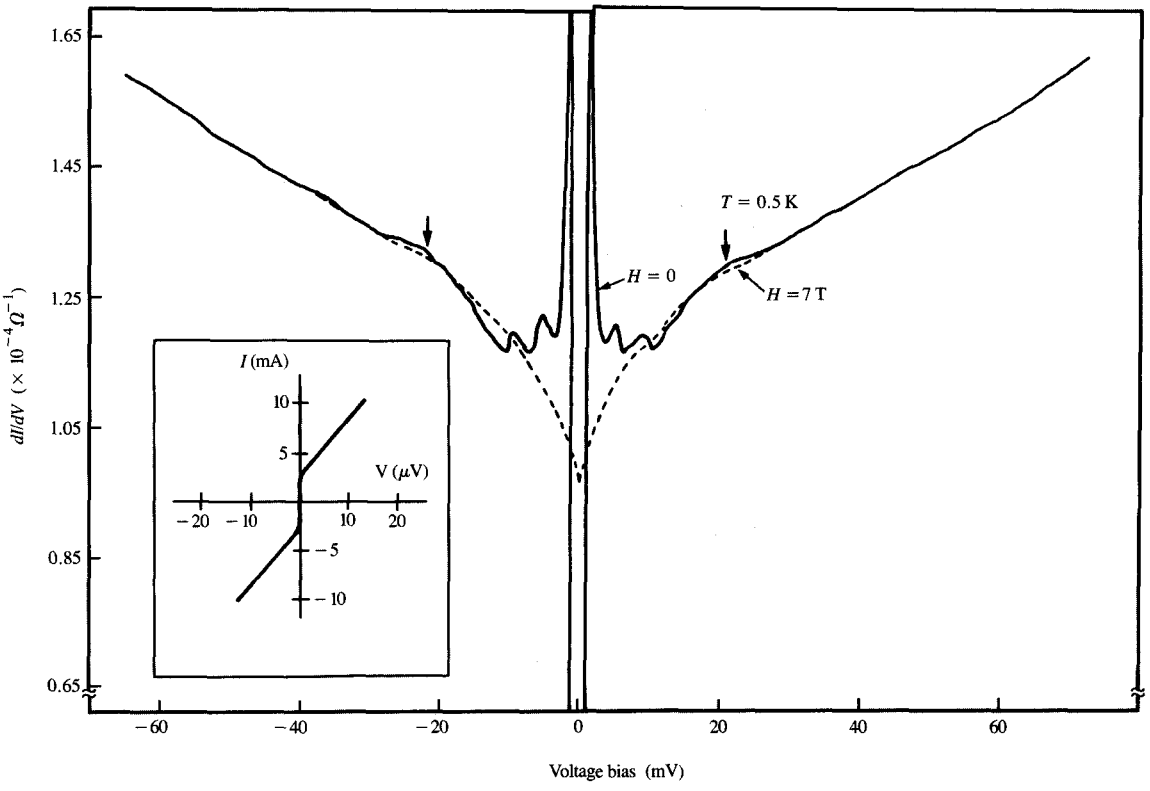

Figure 7

dI/dV of a representative junction in zero field and in 7 T at 0.5 K. No change in the conductance was seen from 0.15 to 7 T. Inset, *I–V* of a shorted junction.

current voltage gives important information on the density of states at the Fermi level.

Figure 7 shows the differential tunneling conductance dI/dV versus bias voltage for a junction formed on a highly oriented *a*-axis YBaCuO thin film using a native barrier and a Pb counter electrode [32]. There is a clear depression of the conductance for bias voltage less than 20 meV, along with clear Pb gap and Pb phonon structure near zero bias. There also is evident a linearly increasing differential conductance at high bias first observed by our group in $(LaSr)_2CuO_4$ films [33]. There is a weak peak above this linear background conductance at about 20 meV. The dashed curve shows the tunneling conductance when superconductivity of the Pb has been quenched by the application of a magnetic field. The picture is certainly one of a very bad junction with strong leakage through which we are probing the Pb gap. If we follow some of these features as a function of temperature, we find that the 20-meV feature disappears at $T_c \approx 60$ K in a BCS fashion. This implies that $2\Delta/kT_c \approx 7$. The slope of the linear conductance as well as its zero bias extrapolation decreases toward T_c and remains constant below T_c. This is certainly in contrast to the prediction of Anderson and Zou [34], who attribute the zero-bias extrapolation to the superfluid density within their RVB model.

It is important to note that in all the tunneling measurements on the 123 phase, T_c as determined from gap opening was found to be 60 K. This is not surprising if we look at the stoichiometry diagram of T_c versus oxygen. The 60 K phase indicates an oxygen-deficient region near the surface [35] that might explain the strong presence of SIN-like tunneling by the Pb counter electrode. Similarly, the existence of a metal–insulator transition, with the possibility of strong electron–electron interaction, may account for the cusp seen at zero bias when the superconductivity in the Pb counter electrode is quenched.

The situation becomes more clear when $Bi_2Sr_2CaCu_2O_8$ single crystals are used. These crystals cleave between the

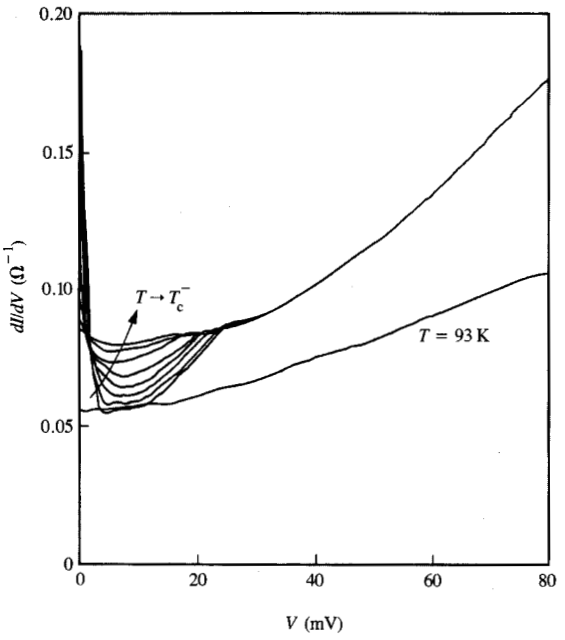

Figure 8

Tunneling spectra dI/dV at various temperatures. The subgap region fills in as T increases toward $T_c \approx 85$ K.

Bi–O layers [36] and form an excellent flat and inert surface. We have deposited Nb as a counter electrode [37]. The result is shown in **Figure 8**. We shall not elaborate on the data, but a few points are in order. First, it is seen that the conductance is no longer linear, but exhibits some curvature. A gaplike feature that follows a BCS temperature dependence with $2\Delta/kT_c \approx 6$–7 is very clear. More details concerning the tunneling data are given in a recent review by Lee et al. [31].

4. Summary

We have described the fabrication of thin films, and their normal-state and superconducting properties.

We have also presented and discussed some topics concerning high-T_c superconductors and have shown the following:

1. The linear resistivity can be explained by ordinary Bloch–Gruneisen behavior and electron–electron interaction.
2. At least down to 80 meV, the carriers in the c-direction behave like free carriers. The anisotropy in the plasma frequencies is about 16.
3. In the superconducting state, the high-T_c materials have a very short coherence length, a feature that affects many material properties, e.g., critical current densities and critical fields.
4. Tunneling data are consistent with $2\Delta kT_c \simeq 6$–7, which is a very strong coupling number compared to that of a theoretical superconductor.

Acknowledgments

The authors are grateful for the collaboration with the Stanford High-T_c group. Many of the results discussed here are part of this continuing effort. This research was supported in part by the National Science Foundation through the Center for Materials Research at Stanford University and by the Air Force Office of Scientific Research.

References

1. K. Char, A. D. Kent, A. Kapitulnik, M. R. Beasley, and T. H. Geballe, *Appl. Phys. Lett.* **51,** 1370 (1987).
2. M. Naito, R. H. Hammond, B. Oh, M. R. Hahn, J. W. P. Hus, P. Rosenthal, A. F. Marshall, M. R. Beasley, T. H. Geballe, and A. Kapitulnik, *J. Mater. Res.* **2,** 713 (1987).
3. A. Kapitulnik, *Proceedings of the International Conference on Materials and Mechanisms of Superconductivity and High Temperature Superconductors*, J. Muller and J. L. Olsen, Eds., *Physica C* **153–155,** 520 (1988).
4. A. Kapitulnik and K. Char, *Proceedings of the International Conference on High Temperature Superconductors*, Trieste, Italy, July 1988, to be published by World Scientific Press, Singapore.
5. K. Char, M. R. Hahn, T. L. Hylton, M. R. Beasley, T. H. Geballe, and A. Kapitulnik, *Proceedings of the International Conference on Applied Superconductivity*, San Francisco, August 1988, to be published.
6. N. Missert, R. H. Hammond, J. E. Mooij, V. Matijasevic, P. Rosenthal, T. H. Geballe, A. Kapitulnik, M. R. Beasley, S. S. Laderman, C. Lu, E. Garwin, and R. Barton, *Proceedings of the International Conference on Applied Superconductivity*, San Francisco, August 1988, to be published.
7. P. M. Mankiewich, J. H. Scofield, W. J. Skocpol, R. E. Howard, A. H. Dayem, and E. Good, *Appl. Phys. Lett.* **51,** 1753 (1987).
8. J. Sizemore, R. Barton, A. F. Marshall, J. C. Bravman, M. Naito, and K. Char, *Proceedings of the International Conference on Applied Superconductivity*, San Francisco, August 1988, to be published.
9. A. F. Marshall, R. W. Barton, K. Char, A. Kapitulnik, B. Oh, R. H. Hammond, and S. S. Laderman, *Phys. Rev. B* **37,** 9353 (1988).
10. K. Char, M. Lee, R. W. Barton, A. F. Marshall, I. Bozovic, R. H. Hammond, M. R. Beasley, T. H. Geballe, A. Kapitulnik, and S. S. Laderman, *Phys. Rev. B* **38,** 834 (1988).
11. H. W. Zandbergen, R. Gronski, and G. Thomas, *Phys. Status Solidi A* **105,** 207 (1988).
12. S. S. Laderman, K. Char, M. Lee, M. R. Hahn, R. H. Hammond, M. R. Beasley, T. H. Geballe, A. Kapitulnik, and R. Barton, submitted to *Phys. Rev. B.*
13. M. Gurvitch and A. T. Fiory, *Phys. Rev. Lett.* **59,** 1337 (1988).
14. J. M. Ziman, *Electrons and Phonons*, Clarendon Press, Oxford, U.K., 1960, p. 364.
15. See for example N. Naito and S. Tanaka, *Proceedings of the Yamada Conference IV, Physics and Chemistry of Layered Materials*, Sendai, Japan, 1980, *Physica B* **105,** 136 (1980).
16. S. W. Tozer, A. W. Kleinsasser, T. Penney, D. Kaiser, and F. Holtzberg, *Phys. Rev. Lett.* **59,** 1768 (1987).
17. N. P. Ong, Z. Z. Wang, S. Hagen, T. W. Jing, J. Clayhold, and J. Horvath, *Physica C* **153–155,** 1072 (1988).
18. Y. Iye, T. Tamegai, H. Takega, and H. Takei, *Jpn. J. Appl. Phys., Series 1, Supercond. Mater.*, p. 46 (1988).

19. Yu. A. Ossipyan, V. B. Timofeev, and I. F. Schegolev, *Physica C* **153–155,** 1133 (1988).
20. I. Bozovic, K. Char, S. J. B. Yoo, A. Kapitulnik, M. R. Beasley, T. H. Geballe, Z. Z. Wang, S. Hagen, N. P. Ong, D. E. Aspnes, and M. K. Kelly, *Phys. Rev. B* **38,** 5077 (1988).
21. D. R. Harshman, G. Aeppli, E. J. Ansaldo, B. Batlogg, J. H. Brewer, J. F. Carolan, R. J. Cava, M. Celio, A. C. D. Chaklader, W. N. Hardy, S. R. Kreitzman, G. M. Luke, D. R. Noakes, and M. Senba, *Phys. Rev. B* **36,** 8850 (1988).
22. C. P. Bean, *Phys. Rev. Lett.* **8,** 250 (1962).
23. B. Oh, M. Naito, S. Arnason, P. Rosenthal, R. Barton, M. R. Beasley, T. H. Geballe, R. H. Hammond, and A. Kapitulnik, *Appl. Phys. Lett.* **51,** 852 (1987).
24. A. P. Malozemoff, T. K. Worthington, Y. Yeshurun, F. Holtzberg, and P. H. Kes, *Phys. Rev. B* **38,** 7203 (1988).
25. W. E. Lawrence and S. Doniach, in *Proceedings of the Twelfth International Conference on Low Temperature Physics*, Kyoto, 1970, Eizo Kanda, Ed., Keigaku, Tokyo, 1971, p. 361.
26. B. Oh, K. Char, A. D. Kent, M. Naito, M. R. Beasley, T. H. Geballe, R. H. Hammond, A. Kapitulnik, and J. M. Graybeal, *Phys. Rev. B* **37,** 7861 (1988).
27. K. Maki, *Prog. Theor. Phys. (Kyoto)* **39,** 897 (1968); R. S. Thomson, *Phys. Rev. B* **1,** 327 (1970).
28. S. Hikami and A. I. Larkin, *Mod. Phys. Lett. B* **2,** 693 (1988).
29. B. Oh, Ph.D. Thesis, Stanford University, Stanford, CA, 1988.
30. For an earlier review, see K. E. Gray, M. E. Hawley, and E. R. Moog, *Proceedings of the Berkeley Conference on Novel Superconductivity*, V. Z. Kresin and S. L. Wolf, Eds., Plenum Press, New York, 1987, p. 611.
31. M. Lee, A. Kapitulnik, and M. R. Beasley, *Proceedings of the NEC Symposium on Mechanisms of High Temperature Superconductivity*, Tokyo, Japan, October 24–27, 1988.
32. M. Lee, M. Naito, A. Kapitulnik, and M. R. Beasley, *Solid State Commun.* (1989), to appear.
33. M. Naito, D. P. E. Smith, M. D. Kirk, B. Oh, M. R. Hahn, K. Char, D. B. Mitzi, J. Z. Sun, D. J. Webb, M. R. Beasley, O. Fischer, T. H. Geballe, R. H. Hammond, A. Kapitulnik, and C. F. Quate, *Phys. Rev. B* **35,** 7228 (1987).
34. P. W. Anderson and Z. Zou, *Phys. Rev. Lett.* **60,** 132 (1988).
35. J. D. Jorgensen, H. Shaked, D. G. Hinks, B. Dabrowski, B. W. Veal, A. P. Paulikas, L. J. Nowicki, G. W. Crabtree, W. K. Kwok, L. H. Hunez, and H. Claus, *Proceedings of the International Conference on Applied Superconductivity*, San Francisco, August 1988, to be published.
36. P. A. P. Lindberg, Z.-X. Shen, B. O. Wells, D. B. Mitzi, I. Lindau, W. E. Spicer, and A. Kapitulnik, *Appl. Phys. Lett.* **53,** 2563 (1988).
37. M. Lee, D. B. Mitzi, A. Kapitulnik, and M. R. Beasley, *Phys. Rev. B* **39,** 801 (1989).
38. T. L. Hylton, M. R. Beasley, A. Kapitulnik, J. P. Carini, L. Drabeck, and G. Gruner, *Proceedings of the International Conference on Applied Superconductivity*, San Francisco, August 1988, to be published.
39. M. J. Ferrari, M. Johnson, F. C. Wellstood, J. Clarke, P. A. Rosenthal, R. H. Hammond, and M. R. Beasley, *Proceedings of the International Conference on Applied Superconductivity*, San Francisco, August 1988, to be published.
40. J. Z. Sun, K. Char, M. R. Hahn, T. H. Geballe, and A. Kapitulnik, *Appl. Phys. Lett.* **54,** 663 (1989).

Received December 29, 1988; accepted for publication February 10, 1989

Aharon Kapitulnik *Department of Applied Physics, Stanford University, Stanford, California 93405.* Professor Kapitulnik served in the Israeli Army from 1973 until 1975 and again in 1978. He received his B.S. (physics) in 1978 and Ph.D. (summa cum laude) in 1983, both from Tel-Aviv University. From 1983 to to 1985, he was a Chaim Weizmann Fellow, an Institute Fellow at the Institute for Polymers and Organic Solids (Department of Physics), and an associate member of the Institute of Theoretical Physics, all at the University of California at Santa Barbara. Professor Kapitulnik was then appointed an assistant professor in residence. He joined the Stanford faculty as an assistant professor of applied physics in 1985, and is currently an Alfred P. Sloan Fellow for the period 1986–1989. In 1987 he was awarded a Presidential Young Investigator grant by the National Science Foundation. Professor Kapitulnik is a member of the American Physical Society.

Kookrin Char *Department of Applied Physics, Stanford University, Stanford, California 93405.* Mr. Char is currently submitting his Ph.D. thesis to the Department of Applied Physics at Stanford University. He received a B.S. degree from Seoul National University in 1982 and the M.S. from the University of California at Los Angeles in 1983.